Probing the Ferredoxin:Hydrogenase Electron Transfer Complex by Infrared Difference Spectroscopy

Selmihan Sahin,[a,b] Johanna Brazard,[c] Takuji B. M. Adachi,[c] Ross D. Milton[a]*, Sven T. Stripp[d]*

[a] University of Geneva, Department of Inorganic and Analytical Chemistry, Sciences II, Quai Ernest-Ansermet 30, 1211 Geneva 4, Switzerland.

[b] Suleyman Demirel University, Department of Chemistry, Faculty of Engineering and Natural Sciences, Cunur, Isparta, 32260 Turkiye.

[c] University of Geneva, Department of Physical Chemistry, Sciences II, Quai Ernest-Ansermet 30, 1211 Geneva 4, Switzerland.

[d] Technische Universität Berlin, Biophysical Chemistry, Strasse des 17. Juni 124, 10623 Berlin, Germany.

ABSTRACT

Ferredoxins are small iron-sulfur proteins that engage in electron transfer (ET) with oxidoreductases across all domains of life. In bacteria, ferredoxins that contain two [4Fe-4S] clusters differ with respect to their electric midpoint potential: while "Alvin"-type ferredoxins show individual potentials between -500 and -650 mV *vs.* SHE, clostridial ferredoxins perform ET at indistinguishable potentials of approximately -400 mV *vs.* SHE. In this work, the electron transfer complex between clostridial ferredoxin *Cp*Fd and [FeFe]-hydrogenases from *Clostridium pasteurianum* (*Cp*I) and green algae *Chlamydomonas reinhardtii* (*Cr*HydA) was investigated spectroscopically. [FeFe]-hydrogenases are oxidoreductases that catalyze hydrogen turnover in bacteria and algae. Introducing the non-canonical amino acid *para*-cyanophenylalanine (pCNF) near to one of the iron-sulfur clusters of *Cp*Fd allowed for a quantification of electric field changes *via* the vibrational Stark effect (VSE) by Fourier-transform infrared (FTIR) spectroscopy. Upon reduction with H_2 or auto-oxidation under N_2, *in situ* FTIR difference spectroscopy reports on protein structural changes. Our data reveal that the affinity between ferredoxin and its redox partners is modulated by redox-dependent protein-protein interactions (PPIs). Prompted by these findings, we discuss whether clostridial ferredoxins might act as two-electron redox partners in contact with hydrogenase or other oxidoreductases.

INTRODUCTION

Protein-protein interactions (PPIs) are central to biochemical reactions[1], including electron transfer (ET) between metalloproteins.[2–4] Small ET proteins such as flavodoxins, blue-copper proteins, and cytochromes[5–7] as well as iron-sulfur proteins[8] serve as redox partners in virtually all metabolic networks. This encompasses photosynthesis and the Calvin-Benson cycle, aerobic respiration and the citric acid cycle, oxidative phosphorylation, and many other redox processes in the cell. For example, the presence of multiple gene copies of iron-sulfur protein ferredoxin has been shown to diversify ET pathways *in vivo*, facilitating discrete reaction couplings, and improve energy conservation mechanisms.[9,10] Moreover, redox state-dependent PPIs optimize the efficiency of ET reactions, particularly if a specific directionality is desired. One example is flavin-based electron bifurcation where high-potential electrons are generated to reduce acceptors such as ubiquinone, pyruvate, NAD(P)H, or others while low-potential electrons are accepted by ferredoxin.[11] Another example is the distribution of electrons *via* ferredoxin and flavodoxin as reduced by Photosystem I during oxygenic photosynthesis.[12] Identifying PPIs is a considerable challenge as most of these interactions are transient and subtle.

Ferredoxins (Fd) are small metalloproteins that engage in ET with various oxidoreductases.[13] They contain either [2Fe-2S] or [4Fe-4S] clusters, depending on their occurrence in eukaryotes or prokaryotes. The primary and secondary coordination sphere of ferredoxin modulates their standard reduction potential (E^0') over hundreds of millivolts[14], which led to the distinction of "low-potential" and "high-potential" ferredoxins.[15] The mesophilic bacterium *C. pasteurianum* produces a low-potential ferredoxin (*Cp*Fd) that contains two [4Fe-4S] clusters (F and F', **Fig. 1**) with similar midpoint potentials (E_m = −400 ±10 mV *vs*. SHE).[16] In contrast, the 2[4Fe-4S] ferredoxin from *A. vinelandii* shows distinct E_ms of −486 mV and −644 mV *vs.* SHE, hinting at two individual one-electron transfer steps.[17] Similar data was reported for the 2[4Fe–4S] ferredoxin from *A. vinosum*, where polar interactions with the clusters were identified to diversify the E_ms.[18] In variance to these "Alvin-type" ferredoxins, often discussed in the context of N_2 fixation[19], Burgess and co-workers have argued that the homogeneity of E_ms in clostridial ferredoxins should allow for both one- and two-electron transfers at the same potential.[17] To the best of our knowledge, however, two-electron reduction of clostridial ferredoxin has not been shown, and it is established that *Cp*Fd likely acts a one-electron carrier functioning at similar E_ms like eukaryotic ferredoxins.[20]

Ferredoxin *Cp*Fd is well-suited for ET with hydrogenase. Hydrogenases are oxidoreductases that catalyze the interconversion of molecular hydrogen (H_2), two protons (H^+), and two electrons (hydrogen turnover).[21,22] In the class of [FeFe]-hydrogenase, catalysis takes place at an unique iron-sulfur-based cofactor, the "hydrogen-forming" H-cluster, which is connect to the protein surface by a proton transfer pathway[23] and an electron relay of up to three [4Fe-4S] clusters.[24–26] The second coordination sphere of standard [FeFe]-hydrogenase is tuned for bidirectional hydrogen turnover.[27] [FeFe]-hydrogenases from *C. pasteurianum* (*Cp*I) or the unicellular green algae *Chlamydomonas reinhardtii* (*Cr*HydA1) are of interest to biotechnological H_2 production, given their high proton reduction rates of up to 10,000 s^{-1}, notably close to the standard potential of hydrogen ($E^{0'}_{2H+/H2}$ = –414 mV *vs.* SHE).[28–30] *In vivo*, [FeFe]-hydrogenase competes for ferredoxin with other oxidoreductases, *e.g.*, in NAD(P)H production, lipid maturation, and N_2 fixation.[31–33] Understanding electron flux in hydrogen turnover, it is important to characterize intermolecular ET between [FeFe]-hydrogenase and ferredoxin, which relies on PPIs[34–36] and, presumably, a successive exchange of single electrons (**Fig. 1**).

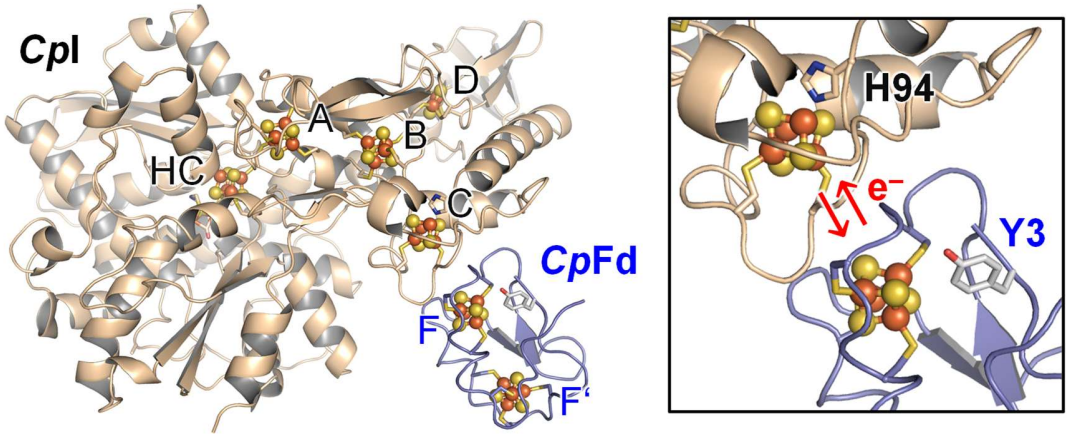

Figure 1. Model of the *Cp*Fd:*Cp*I electron transfer complex. Cartoon representations of [FeFe]-hydrogenase *Cp*I (tan, PDB ID 6N59) containing [4Fe-4S] clusters A–C, [2Fe-2S] cluster D, and the H-cluster (HC). Ferredoxin *Cp*Fd (blue, PDB ID 1CLF) binds two [4Fe-4S] clusters F and F', apart by <9 Å. Inset: the distance between clusters C and F in this model is ~8 Å, in agreement with efficient ET. Note the histidine ligand of cluster C, H94. In this study, tyrosine Y3 of *Cp*Fd is mutated to cyano-phenylalanine (pCNF) as a Stark probe. Model generated with ClusPro 2.[37]

An analytical technique often exploited to investigate PPIs is Fourier-transform infrared (FTIR) spectroscopy, mainly due to its sensitivity detecting small changes in the hydrogen-bonded C=O and N-H groups of the peptide backbone that are informative of secondary structural changes.[38] However, the spectral overlap with solvent (H_2O) complicates the analysis, in particular when transient and/or subtle changes are addressed. These challenges can be overcome by FTIR difference spectroscopy where the activity of a sample is induced by a specific trigger (light, potential jumps, reactant titrations, etc.) that allow analyzing the spectral *changes* rather than the absolute spectra.[39–43]

Introducing specific chromophores by protein engineering is a complementary strategy. Here, the reporter group shows favorable spectroscopic properties like a high extinction coefficient or a distinct absorption frequency. This can be achieved by amber codon suppression using an aminoacyl-tRNA synthetase/tRNA pair designed for the selective insertion of non-canonical amino acids.[44] A common example is the use of 4-cyano-L-phenylalanine (pCNF), which contains an IR-active nitrile group (-C≡N) that can be probed to measure changes in the electric field *via* the vibrational Stark effect (VSE).[45–47] The VSE originates from the small differences in dipole moment between the first vibrationally exited state ν_1 compared to the ground state ν_0. An external electric field, *e.g.*, as projected onto the nitrile group by the protein environment, interacts differently with the ν_1 or ν_0 dipole moment.[48] The measured frequency shift $\Delta\nu$ is then proportional to the electric field vector $\vec{F}$ with the negative difference in dipole moments $\Delta\vec{\mu}$, the later which is also referred to as Stark tuning rate. The introduction of pCNF within a protein yields a local electric field probe.[49]

To investigate the changes in redox state of ferredoxin *Cp*Fd under turnover conditions we replaced tyrosine Y3 by the non-canonical amino acid pCNF near the [4Fe-4S] cluster F (**Fig. 1**). With the aim of minimizing any other changes to *Cp*Fd, we targeted the only tyrosine residue of the protein. The *Cp*Fd:*Cp*I docking model presented in **Fig. 1** indicates that the pCNF residue may be positioned 6.5–8.5 Å from the *Cp*Fd:*Cp*I interface, and that the distal [4Fe-4S] cluster of *Cp*I (C) may be 11–12.5 Å away. We expect that changes in redox state give rise to a VSE at the nitrile group. Additionally, we used *in situ* attenuated total reflectance (ATR) FTIR difference spectroscopy to investigate *Cp*Fd in complex with [FeFe]-hydrogenases *Cp*I or *Cr*HydA1, triggering reduction and oxidation by changing the gas atmosphere between H_2, N_2, or O_2. A subtle

yet significant shift of the nitrile band was observed, accompanied by clear changes in protein secondary structure. These differences are attributed to structural changes at the *Cp*Fd:*Cp*I interface that modulate the ET dynamics between ferredoxin and hydrogenase.

MATERIALS AND METHODS

Strains, plasmids, and reagents. Amber codon suppression was performed using *Escherichia coli* strain C321.ΔA.opt, in which all amber codons have been re-coded (strain C321.ΔA.opt was a gift from George Church, Addgene plasmid #87359).[50] Site-specific pCNF insertion by amber codon suppression was performed using the aminoacyl tRNA synthetase/tRNA pair offered by the plasmid pDule2-pCNF, a gift from Ryan Mehl (Addgene plasmid #85495).[51] Initial pCNF incorporation tests were performed using plasmid pBAD-sfGFP 150TAG, where induction using arabinose yields superfolder green fluorescent protein ("sfGFP") containing the pCNF residue at position 150. This plasmid was linearized by PCR and a synthetic gene encoding wild-type *Cp*Fd carrying a *C*-terminal Strep-tag "WSHPQFEK" (codon optimized, ThermoFisher Scientific Switzerland) was inserted by Gibson assembly to yield plasmid pBAD-*Cp*Fd. pBAD-sfGFP 150TAG was a gift from Ryan Mehl (Addgene plasmid #85483).[52] Note that the Step-tag includes a *C*-terminal tryptophan residue (W) which is not expected to impact the *Cp*Fd:*Cp*I complex (**Fig. S1**). Site-directed mutagenesis was performed using Gibson assembly to replace the codon corresponding to Y3 of *Cp*Fd (TAT) with the TAG amber stop codon, yielding plasmid pBAD-*Cp*Fd-Y3pCNF. The unnatural amino acid pCNF was purchased from Bachem (Switzerland, product 4028063, H-4-cyano-Phe-OH). Unless stated otherwise, all chemicals were purchased from Sigma Aldrich, Inc. (Switzerland) and used without further purification. PCR was performed with Phusion High Fidelity DNA polymerase (Thermo Fisher Scientific Switzerland). Site directed mutagenesis was performed with GeneArt Gibson Assembly HiFi Master Mix (Thermo Fisher Scientific Switzerland) using the specific Gibson primers. Plasmid DNA isolation was performed with the Nucleobond Xtra Mini Kit (Macherey-Nagel, Switzerland). Oligonucleotides were supplied by Microsynth (Switzerland).

Cell growth and protein Purification. *E. coli* C321.ΔA.Opt was chemically transformed with the plasmid pBAD-*Cp*Fd for the production of wild-type *Cp*Fd. To produce pCNF-containing *Cp*Fd, plasmid pBAD-*Cp*Fd-Y3pCNF was chemically co-transformed (sequentially) with plasmid pDule2-pCNF into *E. coli* C321.ΔA.opt cells; successful transcription, translation, and TAG-suppression yields Y3pCNF-*Cp*Fd, where the Tyr3 amino acid has been replaced with pCNF. Glycerol stocks of transformed cells were prepared and kept at −80 °C for further studies.

Starter cultures of the transformed cells were individually prepared in 60 mL of LB-Miller medium supplemented with ferric ammonium citrate (2 mM) and MOPS/NaOH buffer (100 mM, final pH of 7.8).[53] Starter cultures were incubated at 30 °C (200 rpm) for 18 h of growth. All cultures/media were supplemented with the relevant antibiotics for plasmid selection: 100 µg/mL ampicillin (for pBAD-X plasmids) and 100 µg/mL spectinomycin for pDule2-pCNF. The starter cultures (60 mL) were used to inoculate 3 L of medium in 5 L baffled flasks. Once the optical density had reached $0.5_{600\ nm}$, expression was induced with the addition of arabinose (final concentration = 0.1 % w/v), cysteine was added (to 2 mM), the temperature was lowered to 25 °C, and incubation under microaerobic conditions was achieved by lowering the rpm to 75, overnight. For the expression of Y3pCNF-*Cp*Fd, pCNF was included in the main culture (1 mM) at the time of induction. All cells were harvested by centrifugation at 4000 x *g* for 20 minutes (ambient temperature).

All purification steps were performed under an anoxic environment (within an anoxic glovebox, >95% N_2/<5% H_2, COY Laboratory Products MI USA). All solutions were equilibrated with the glovebox atmosphere by stirred for 24 h. For protein purification, the obtained cell paste was resuspended in "Buffer A" (50 mM potassium phosphate/NaOH buffer, pH 7.0, containing 150 mM NaCl and 0.5 mM DT) containing ~2 µg/mL DNAse A and 1 mg/mL of lysozyme. The resuspended cells were lysed anaerobically by sonication (10 min, 2 sec ON, 2 sec OFF, 50% Amplitude, Fisherbrand FB120) and the cell lysate was clarified by centrifugation at 30,000 x *g* for 1 h at 4 °C to remove cell debris. The supernatant was then filtered through a 0.45 µm syringe filter, and loaded onto a Strep column (StrepTrap XT, 5 mL, Cytiva), pre-equilibrated with 50 mM phosphate/NaOH buffer (pH 7.0 containing 150 mM NaCl and 0.5 mM DT). The column was then washed with 3 column volumes of Buffer A. The wild-type *Cp*Fd or Y3pCNF-*Cp*Fd was subsequently eluted using Buffer A containing 50 mM biotin (Chemodex). The eluted protein was next desalted using a HiPrep 26/10 desalting column pre-equilibrated with Buffer A to remove

excess biotin. The eluted proteins were concentrated using an Amicon stirred concentrator cell (Merck-Millipore) equipped with a 3 kDa microfilter. The concentrated protein was then stored as 10 µL pellets in liquid nitrogen until further use. Protein concentrations of the preparations were estimated using a molar absorptivity of $\varepsilon_{390} = 30\ mM^{-1}\ cm^{-1}$ and relative iron-sulfur cluster content was estimated considering the ratio $A_{390\ nm}/A_{280\ nm}$ for *Cp*Fd which had oxidized in air.[54]

[FeFe]-hydrogenase *Cp*I was produced as reported previously.[53] In brief, *Cp*I carrying a C-terminal Strep-tag was heterologously produced in *E. coli* BL21 *ΔiscR* carrying plasmid pACYC-hydEF-hydGX for the co-expression of [FeFe]-hydrogenase-specific maturases HydEFG.[55]

Fluorescence Measurements. Fluorescence emission spectra were recorded on a TECAN infinite M Nano+ absorbance plate reader using a black plate with an integration time of 20 µs nm^{-1}, a resolution of 2 nm, and an excitation slit width of 5 nm. The excitation wavelength of pCNF (50 µM) was determined by scanning the wavelength range of 230–260 nm, where the maximum excitation wavelength was determined as 238 nm. Fluorescence emission spectra were recorded between 280 nm and 450 nm by exciting 10 µM protein samples in 0.1 M MOPS/NaOH buffer (pH 7.0) at 238 nm. For urea-unfolded protein spectra, the protein samples were treated with 8 M urea for 2 h at 37 °C.

Vibrational spectroscopy. Raman spectra of wild-type *Cp*Fd and Y3pCNF-*Cp*Fd were recorded at room temperature, using a home-built microspectroscopy setup as described previously.[56] The excitation source was a 532 nm CW laser (Laser Quantum, Opus 532). The laser beam was depolarized using a liquid crystal polymer depolarizer (Thorlabs, DPP25-A). The beam was reflected by a dichroic beamsplitter (AHF Analysentechnik AG, Raman beamsplitter RT 532 rdc). The beam was focused at 50 µm from the glass substrate into a sample by the water-immersion objective lens (Olympus UPLSAPO60XW, NA=1.2). The laser power was ~20 mW after the objective lens. The collected signal was spatially filtered at the conjugate plane using a 50 µm pinhole and a 532 nm RazorEdge ultrasteep long-pass filter (Semrock, LP03-532RE-25) was used to remove the excitation beam from Raman scattering. Raman spectra were acquired by using a spectrograph (Andor, Kymera 328) with an EMCCD (Andor, Newton 970). Each spectrum was recorded by averaging seven spectra with the exposure time of 360 s (total accumulated time of 42 min). The averaged spectra were smoothed by using a Savitzky-Golay filter. 10 µL of the protein in buffer (~1 mM) was deposited on a clean cover glass with a silicone isolator sheet (0.25 mm

thick, Grace Bio-Labs 664475) with a 10 mm hole. The samples were sealed by adding a cleaned cover glass on top of the silicone isolator sheet.

Infrared spectroscopy on *Cp*Fd and [FeFe]-hydrogenases *Cp*I and *Cr*HydA1 was performed on hydrated protein films in attenuated total reflection (ATR) configuration using a FTIR spectrometer (Bruker Tensor27) equipped with an MCT detector cooled by liquid N_2.[43] All data were recorded with a spectral resolution of 2 cm^{-1} at 80 kHz scanning velocity. For 50 co-additions of interferometer scans in forward/backward direction, a temporal resolution of 10 s was achieved. Steady-state spectra represent co-addition of up to 1.000 interferometer scans. All experiments were conducted under 1 atm N_2, at ambient temperature, and in the dark. Reduction of *Cp*I was triggered by introducing 10% H_2 in the gas phase while pure N_2 induced catalytic "auto-oxidation" of *Cp*I. In the presence of 10% O_2, the [FeFe]-hydrogenase was deactivated.[57] The redox-dependent pCNF frequency shifts were analyzed comparing second derivative absolute spectra as calculated in OPUS (Bruker). Secondary structural changes in the *Cp*Fd:*Cp*I complex were evaluated by subtracting spectra under N_2 from spectra under 10% H_2 (in the presence of H_2O or D_2O).

Protein film electrochemistry. All electrochemical measurements were performed by using an AUTOLAB PGSTAT101 controlled by NOVA (Metrohm Suisse), connected to an anoxic Ar glove box (< 1 ppm O_2, Jacomex, France). *Cp*Fd and Y3pCNF-*Cp*Fd bioelectrodes were prepared by drop-casting 2 µL of either protein (250 µM stock solutions) on 3 mm diameter graphite rod electrodes (0.07 cm^{-2}, prepared by heat-shrink insulating walls of the electrode). The electrodes were left to dry at room temperature for 10 min. All cyclic voltammograms (CVs) were recorded in 25 mM potassium phosphate/NaOH buffer (pH 7.5, containing 0.1 M NaCl and 50 mM $MgCl_2$) using a scan rate of 25 mV/s alongside a platinum wire counter electrode and a saturated calomel electrode (SCE) as the reference electrode. All potentials were converted to the standard hydrogen electrode (SHE) according to $E_{SHE} = E_{SCE} + 0.242$ V. GNU Octave was used to remove the background applying a sixth-order spline.

RESULTS AND DISCUSSION

The production of holo-*Cp*Fd (wild type) and holo-Y3pCNF-*Cp*Fd in *E. coli* C321.ΔA.opt was confirmed by electronic spectroscopy, where one broad band at ~400 nm reflects the presence of

the oxidized [4Fe-4S] clusters (**Fig. 2A**).[58] In comparison to wild-type *Cp*Fd, the total protein yield of Y3pCNF-*Cp*Fd decreased five-fold. This can be explained by translation stalling until the arrival of the pCNF-charged tRNA, or by a low cytoplasmic concentration of free pCNF. Importantly, the production of Y3pCNF-*Cp*Fd was also found to decrease by a further five-fold in the absence of pCNF in the culture medium, confirming the selectivity of the orthogonal aminoacyl-tRNA synthetase/tRNA pair for tRNA charging with pCNF.

The incorporation of pCNF was first verified by fluorescence spectroscopy. Cyano-phenylalanine is of interest due to improved molar absorptivity and fluorescence quantum yield over tryptophan (W) or tyrosine (Y), serving as an optical probe to characterize conformational changes in proteins.[54] However, if the distance between W/Y and pCNF is sufficiently small, fluorescence quenching through Förster Resonance Energy Transfer (FRET) occurs.[59,60] In the case of Y3pCNF-*Cp*Fd, the only Y residue of the protein was replaced with pCNF but a *C*-terminal W residue was introduced as part of the Strep-tag. A prediction of the tertiary structure of Y3pCNF-*Cp*Fd by AlphaFold (**Fig. S1**) suggests that the distance between pCNF and W could be as little as 7.6 Å; a suitable distance for FRET. **Figure S2** reports the fluorescence emission of the pCNF residue of Y3pCNF-*Cp*Fd, where protein unfolding in the presence of 8 M urea results in an increase of fluorescence emission of pCNF. This is consistent with quenching of pCNF emission when the protein is in a folded state and pCNF is presumably closer to W than in the unfolded state. The increase in fluorescence emission can also be explained by an increase in solvation of the pCNF residue upon protein unfolding. An unspecific increase in the fluorescence emission of Y3pCNF-*Cp*Fd, *i.e.*, in the absence of 8 M urea, was not observed (**Fig. S2**).[51]

We next determined whether the presence of pCNF induces a significant change in E^0' of its neighboring [4Fe-4S] cluster using protein film voltammetry (**Fig. 2B**). Due to either *(i)* fast intermolecular ET between the [4Fe-4S] clusters of *Cp*Fd or (*ii*) electronically similar environments around the [4Fe-4S] clusters (<9 Å apart), a single pair of redox peaks at −0.390 ± 0.007 V *vs.* SHE was observed, in good agreement with previous investigations.[61,62] In the case of the Y3pCNF-*Cp*Fd, a single pair of redox peaks was observed at −0.378 ± 0.016 mV *vs*. SHE, suggesting that the presence of pCNF did not introduce a significant change in E_m (Student's *t* test, $P = 0.0996$).

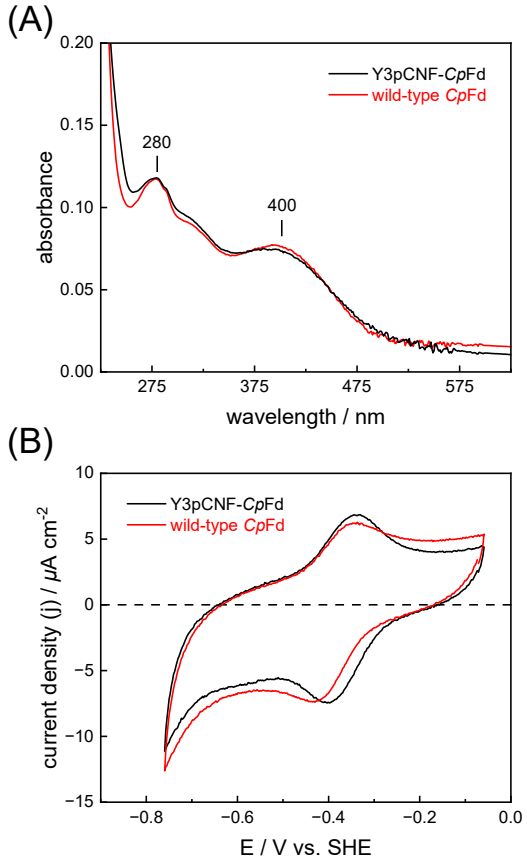

Figure 2. Electronic spectroscopy and protein film electrochemistry. (A) Electronic spectra of wild-type *Cp*Fd (red) and Y3pCNF-*Cp*Fd (black) recorded in aerobic MOPS/NaOH buffer (0.1 M, pH 7) at 25 °C. The broad band at 400 nm shows the presence of oxidized iron-sulfur clusters ($[4Fe\text{-}4S]^{2+}$). **(B)** Representative cyclic voltammograms of wild-type *Cp*Fd (red) and Y3pCNF-*Cp*Fd (black) recorded in aerobic potassium phosphate/NaOH buffer (25 mM pH 7.5, 0.1 M NaCl, and 50 mM $MgCl_2$) at 25 °C with a scan rate of 25 mV/s.

The incorporation of pCNF was then verified by two independent vibrational spectroscopic approaches. Raman spectra reveal a single band at 2234 cm^{-1} that is exclusively observed in the Y3pCNF-*Cp*Fd sample and can be assigned to the nitrile stretching vibration of pCNF (**Fig. S2**). The relatively high frequency and broad band shape suggests hydrogen-bonding with the solvent.[49] Independent confirmation was achieved by FTIR spectroscopy (**Fig. 3A**). Interestingly, we found that the pCNF band position shifted by 4–5 cm^{-1} toward lower frequencies when water was removed from the protein film (**Fig. S3**), in agreement with a progressive lack of hydrogen-bonding

interactions upon dehydration. Therefore, any comparison must be performed under unchanging hydration levels. No meaningful nitrile shifts were detected upon electrochemical reduction of Y3pCNF-*Cp*Fd, in the presence of dithionite, or upon oxidation with O_2 (**Fig. S4**).

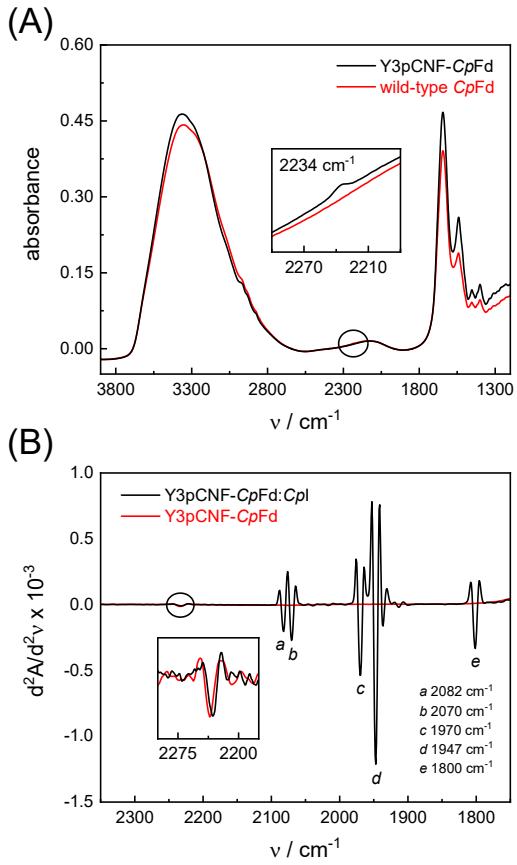

Figure 3. Steady-state vibrational spectroscopy. (A) ATR FTIR spectra of wild-type *Cp*Fd (red) and Y3pCNF-*Cp*Fd (black) confirming the presence of the nitrile band of pCNF at ~2234 cm^{-1} (inset). **(B)** Second derivate FTIR spectra of the Y3pCNF-*Cp*Fd:*Cp*I complex (black) show five strong bands (a)–(e) between 2150–1750 cm^{-1} that have been assigned to the diatomic ligands of the H-cluster in the oxidized resting state H_{ox}. These bands are missing in the Y3pCNF-*Cp*Fd spectrum (red); however, at higher frequencies both spectra show the nitrile band of pCNF (inset). In complex with *Cp*I, this band is red-shifted by 3–4 cm^{-1} relative to *Cp*Fd.

To probe the reduction and oxidation of Y3pCNF-*Cp*Fd under turnover conditions, we mixed the protein with its natural redox partner, the [FeFe]-hydrogenase *Cp*I [63], in a ratio of 5:1. The second derivative FTIR spectrum shows that the nitrile band is found at ~2230 cm^{-1} (**Fig. 3B**), suggesting complex formation between *Cp*I and *Cp*Fd and less solvent access around Y3pCNF. At lower frequencies, the spectrum reveals strong absorbance bands (a)–(e) that have been assigned to the cyanide (CN^-) and carbon monoxide (CO) ligands of *Cp*I.[28–30] The IR signature is characteristic for the oxidized resting state of the H-cluster, H_{ox}, and unaffected by the presence of *Cp*Fd.

We hypothesize that reduction and oxidation of *Cp*I may result in ET with Y3pCNF-*Cp*Fd.[34–36] Therefore, the Y3pCNF-*Cp*Fd:*Cp*I protein film was probed in the presence of N_2, H_2, or O_2 employing our unique setup for *in situ* ATR FTIR spectroscopy.[43] For this, 1 µL protein solution was concentrated on the ATR crystal under a stream of dry N_2 and re-hydrated with N_2 aerosol until the protein film adopted an equilibrium with the humidity in the gas phase. Five N_2/H_2 cycles followed by incubation with O_2 were performed, where a treatment with O_2 at the end of the experiment deactivates *Cp*I – [FeFe]-hydrogenases are oxygen-sensitive[57] – ultimately impeding H_2 oxidation and subsequent ET toward Y3pCNF-*Cp*Fd. **Figure 4A** illustrates how H_{ox} converts into redox states H_{red} and H_{sred} under 10% H_2[64], auto-oxidation in the absence of H_2 (100% N_2), and oxygenic deactivation of *Cp*I in the presence of 10% O_2. **Figure 4B** shows second derivative spectra of the Y3pCNF-*Cp*Fd:*Cp*I film in the energy regime of the pCNF nitrile band (same data set as in **Fig. 4A**). We observe a distinct up-shift from 2229.5 ± 0.15 cm^{-1} to 2231.3 ± 0.15 cm^{-1} in the presence of 10% H_2 ($\Delta\nu = 1.8\ cm^{-1}$) that is reversible when the gas atmosphere is switched back N_2. With a Stark tuning rate of 0.71 cm^{-1}/MV/cm for pCNF[65], this is equivalent to a local electric field change of +2.53 mV/cm. Plotting the band position against gas treatment, **Fig. 4C** illustrates that once *Cp*I is deactivated with 10% O_2, subsequent treatment with H_2 no longer impacts the nitrile band. Significant hydration changes that would affect the nitrile frequency were avoided (**Fig. 4D** and **Fig. S3**).

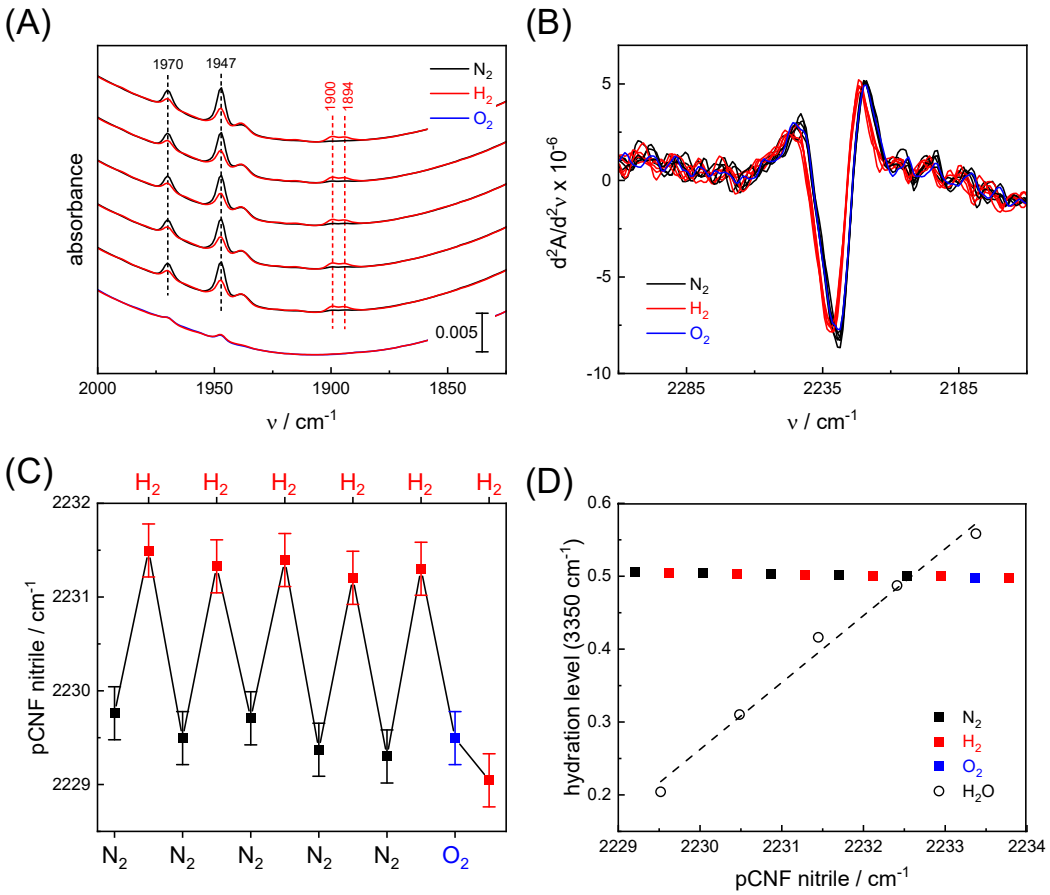

Figure 4. ***In situ*** **analysis of the ferredoxin:hydrogenase complex. (A)** ATR FTIR spectra of the H-cluster's CO ligands show the repeated reduction under 10% H_2 (increase of H_{red} and H_{sred} at 1900 and 1894 cm^{-1}, respectively) and oxidation under N_2 (H_{ox} at 1970 and 1947 cm^{-1}). In the presence of 10% O_2, all CO bands disappear due to disintegration of the H-cluster. **(B)** Second derivative ATR FTIR spectra of the Y3pCNF-*Cp*Fd:*Cp*I complex in the frequency regime of the nitrile band under N_2 (black), 10% H_2 (red), or 10% O_2 (blue). **(C)** The shift of the nitrile band as a function of gas composition. After deactivation of *Cp*I with O_2, a reaction with H_2 is no longer observed. **(D)** Shift of the nitrile band as a function of hydration level (measured at 3350 cm^{-1}, compare **Fig. S3**). The pCNF up-shift for increasingly humid protein films can be followed by linear regression (dashed line). In comparison, the unchanging hydration level in the $N_2/H_2/O_2$ titration allows excluding any unspecific effects.

Whether the nitrile shift is a general feature of ferredoxin reduction or specific to the complex with *Cp*I can be probed in presence of *Cr*HydA1 as an alternative [FeFe]-hydrogenase. The so-called minimal [FeFe]-hydrogenase *Cr*HydA1 lacks the iron-sulfur cluster domain of *Cp*I but has been demonstrated to interact with both plant-type and bacterial ferredoxins.[66–68] Surprisingly, however, a nitrile shift was not observed when the Y3pCNF-*Cp*Fd:*Cr*HydA1 complex was reacted with H_2 (**Fig. S5**). We speculate that the changes observed for the pCNF nitrile band are due to protein structural changes in the Y3pCNF-*Cp*Fd:*Cp*I complex and PPI-coupled ET events specific for the interaction with the F-domain of *Cp*I.

To investigate redox-dependent protein structural changes, FTIR difference spectra of Y3pCNF-*Cp*Fd in complex with *Cp*I or *Cr*HydA1 were analyzed. For these data, spectra under N_2 were subtracted from spectra under 10 % H_2 ("H_2–N_2") recorded in a time-dependent fashion in the same experimental setup. **Figure 5A** shows the temporal evolution of H_2–N_2 difference spectra for Y3pCNF-*Cp*Fd:*Cp*I, 10–50 s after initial contact with H_2. Between 2150–1750 cm^{-1}, negative bands (a)–(e) indicate depletion of the oxidized H-cluster (H_{ox}, as accumulated under N_2) while positive bands (f)–(j) indicate evolution of the one-electron reduced H-cluster state H_{red} in the presence of H_2 (**Tab. S2**).[64] Below 1700 cm^{-1}, the spectra show differential signals at 1670 and 1624 cm^{-1} as well as 1574 and 1548 cm^{-1}. A negative band pattern becomes visible around 1515 cm^{-1}. The prominent 1670/1624 feature can be assigned to secondary structural changes involving the amide I band, *i.e.*, a formation of β-sheets over random coil structures.[38] As the amide I band is dominated by the C=O stretching frequency of the protein backbone, the lack of spectral shifts in D_2O agrees with this assignment (**Fig. S6**). Smaller features between 1600–1500 cm^{-1} might stem from amide II changes; however, no significant downshifts were observed upon deuteration (**Fig. S6**). The assignment of the complex band pattern around 1515 cm^{-1} is unclear. Whether such protein structural changes can be assigned to hydrogenase, ferredoxin, or both will be clarified in future studies, *e.g.*, producing one protein from a ^{13}C source.[69]

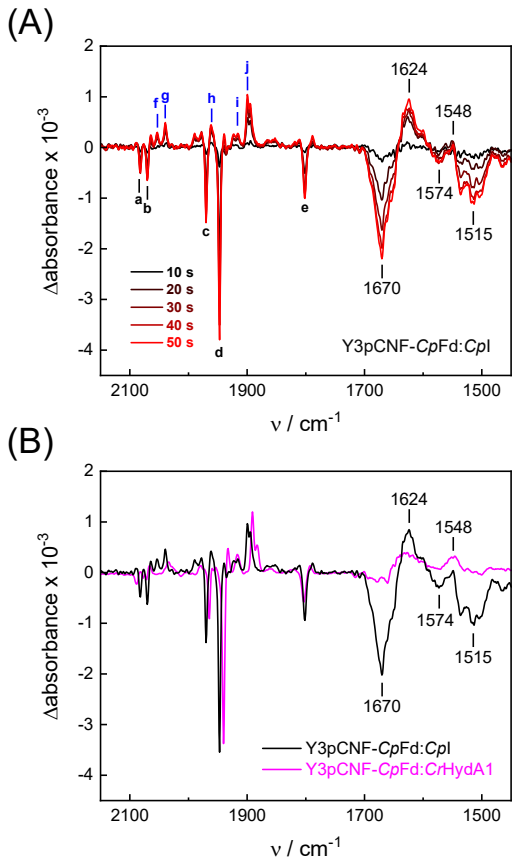

Figure 5. Infrared difference spectroscopy. (A) Time series of H_2–N_2 ATR FTIR difference spectra of Y3pCNF-*Cp*Fd:*Cp*I between 10–50 s. Bands above 1750 cm^{-1} are assigned to H-cluster ligands in the H_{ox} state (a)–(e) and H_{red} state (f)–(j). Additionally, the spectrum includes reduced states H_{sred} and H_{hyd} (**Fig. S3**). At lower frequencies, the 1670/1624 feature indicates protein structural changes. **(B)** Comparison of *Cp*Fd in complex with either *Cp*I (black) or *Cr*HydA1 (magenta), normalized to H_{ox} band d. Note the lack of the 1670/1624 feature in the Y3pCNF-*Cp*Fd:*Cr*HydA1 complex. The small differences between the H-cluster bands of *Cr*HydA1 and *Cp*I in the oxidized and reduced states is a known feature and unrelated to the presence of ferredoxin.

Remarkably, when the Y3pCNF-*Cp*Fd:*Cr*HydA1 complex was reduced with H_2 band changes below 1700 cm^{-1} were nearly absent (the magenta-colored traced in **Fig. 5B** only show small positive bands for amide I and amide II due to an unspecific decrease in film hydration), and not detected at all when *Cr*HydA1 was reduced in the absence of *Cp*Fd (**Fig. S6**). **Figure 5** thus provides conclusive evidence of how PPIs and protein structural changes are specific for the complex between *Cp*Fd and *Cp*I as [FeFe]-hydrogenase *Cr*HydA1 shows only a fraction of the

1670/1624 feature. This observation is explained with the unique ferredoxin interface of *Cr*HydA1 [35] and the lack of the F-domain and its iron-sulfur clusters.[67] In activity assays, *Cp*Fd and *Cr*HydA1 have been shown to interact, so we have no reason to assume that the bacterial ferredoxin cannot receive electrons from the algal hydrogenase.[66–68] The lack of significant nitrile shifts upon reduction of the Y3pCNF-*Cp*Fd:*Cr*HydA1 complex (**Fig. S5**) therefore indicates that the pCNF residue indeed senses specific structural changes in the Y3pCNF-*Cp*Fd:*Cp*I complex. Here, the electric field change of +2.53 mV/cm is small, but in agreement with literature.[70–72] In future work, we will explore this interpretation by calculating the VSE from QM/MM simulations of the oxidized and reduced ferredoxin:hydrogenase complex.

In general, the observed up-shift upon reduction indicates an accumulation of negative charge in front of the nitrile N-atom. Based on our docking model (**Fig. 1**), this may also hint at a reduction of the nearest [4Fe-4S] cluster in the F-domain of *Cp*I. Artz *et al.* have argued that [4Fe-4S] cluster C controls hydrogenase activity due to its low $E^{0'}$ of approximately –450 mV vs SHE, functioning as a "gate keeper" for catalytic ET.[34] This interpretation agrees with the lack of changes in the *Cp*Fd:*Cr*HydA1 complex where ferredoxin would interact with the H-cluster directly.

CONCLUSIONS

We present a dynamic analysis of the electron transfer complex between ferredoxin *Cp*Fd and structurally diverse [FeFe]-hydrogenases *Cp*I and *Cr*HydA1. The introduction of the non-canonical amino acid pCNF as a Stark probe allowed the estimation of electric field changes upon reduction or oxidation of the complex, and FTIR difference spectroscopy uncovered pronounced protein structural changes. Such dynamic behavior is rarely picked up in structural biology, although the "sampling" of different conformations in cryogenic electron microscopy (cryo EM) may lead to respective findings.[73–75] Our observations can explain the typically superior performance of hydrogenases with ferredoxin over general reductants: (*i*) the specificity of contact secures optimal ET distances, and (*ii*) the dynamic changes at the ET interface allow dissociation of the complex once ET has taken place. This way, the two-electrons chemistry of hydrogenase is efficiently promoted by a one-electron redox partner like ferredoxin. Recent data from Steinhilper *et al.* suggests that similar principles may apply to other ferredoxin-driven redox processes as well.[76]

All things considered, it is worth reflecting whether concerted two-electron redox chemistry with 2[4Fe-4S]-type ferredoxins can be strictly excluded. Our data suggests that a change in protein conformation may occur once ET has taken place; from this, we speculate that PPIs in the *Cp*Fd:*Cp*I complex may be favored when redox states are complementary, *i.e.*, oxidized *Cp*I may "select" for reduced *Cp*Fd, and *vice versa*. We also speculate that a single interaction between *Cp*I and *Cp*Fd may function to transfer a total of two electrons, given that the two [4Fe-4S] clusters are of similar potential and situated within a distance that is widely accepted to lead to physiologically relevant ET[77], similar to the situation within the iron-sulfur cluster network of *Cp*I.[78]

ASSOCIATED CONTENT

Supporting Information. Evaluation of the *Cp*Fd:*Cp*I complex model, fluorescence and Raman spectra, additional infrared spectra. This material is available free of charge *via* the Internet at http://pubs.acs.org.

AUTHOR INFORMATION

Corresponding Author

* Ross D. Milton (ross.milton@unige.ch) and Sven T. Stripp (s.stripp@tu-berlin.de)

Author Contributions

The manuscript was written through contributions of all authors. All authors have given approval to the final version of the manuscript.

Funding Sources

S. Sahin acknowledges funding from a Marie Curie-Skłodowska Individual Fellowship under the European Union's Horizon 2020 research and innovation program (101024443, "BERCO2"). Ross D. Milton acknowledges the Swiss National Science Foundation (200021_191985) for support. Sven T. Stripp acknowledges funding by the German Research Foundation priority program 1927 (STR1554/5-1). Takuji B. M. Adachi acknowledges the Société Académique de Genève and Fondation Ernst et Lucie Schmidheiny for financial support.

ACKNOWLEDGMENTS

We thank Alexandre Jolly for assistance with pCNF-containing protein expression. We acknowledge Dr. Jacek Kozuch, Prof. Esteban Vöhringer-Martinez, and Dr. Rodrigo Recabarren for discussing the effect of electric field changes within proteins.

REFERENCES

(1) Keskin, O.; Gursoy, A.; Ma, B.; Nussinov, R. Principles of Protein−Protein Interactions: What Are the Preferred Ways For Proteins To Interact? *Chem Rev* **2008**, *108* (4), 1225–1244. https://doi.org/10.1021/cr040409x.

(2) Gray, H. B.; Winkler, J. R. Electron Transfer in Proteins. *Annu Rev Biochem* **1996**, *65*, 537–561. https://doi.org/https://doi.org/10.1146/annurev.bi.65.070196.002541.

(3) Gray, H. B.; Winkler, J. R. Long-Range Electron Transfer. *Proc Natl Acad Sci U S A* **2005**, *102* (10), 3534–3539. https://doi.org/10.1073/pnas.0408029102.

(4) Dempsey, J. L.; Winkler, J. R.; Gray, H. B. Proton-Coupled Electron Flow in Protein Redox Machines. *Chem Rev* **2010**, *110* (12), 7024–7039. https://doi.org/10.1021/cr100182b.

(5) Sancho, J. Flavodoxins: Sequence, Folding, Binding, Function and Beyond. *Cell Mol Life Sci* **2006**, *63* (7–8), 855–864. https://doi.org/10.1007/s00018-005-5514-4.

(6) De Rienzo, F.; Gabdoulline, R. R.; Menziani, M. C.; Wade, R. C. Blue Copper Proteins: A Comparative Analysis of Their Molecular Interaction Properties. *Protein Science* **2000**, *9* (8), 1439–1454. https://doi.org/10.1110/ps.9.8.1439.

(7) Alvarez-Paggi, D.; Hannibal, L.; Castro, M. A.; Oviedo-Rouco, S.; Demicheli, V.; Tórtora, V.; Tomasina, F.; Radi, R.; Murgida, D. H. Multifunctional Cytochrome *c* : Learning New Tricks from an Old Dog. *Chem Rev* **2017**, *117* (21), 13382–13460. https://doi.org/10.1021/acs.chemrev.7b00257.

(8) Beinert, H. Iron-Sulfur Proteins: Ancient Structures, Still Full of Surprises. *J Biol Inorg Chem* **2000**, *5* (1), 2–15.

(9) Peden, E. A.; Boehm, M.; Mulder, D. W.; Davis, R.; Old, W. M.; King, P. W.; Ghirardi, M. L.; Dubini, A. Identification of Global Ferredoxin Interaction Networks in Chlamydomonas Reinhardtii. *Journal of Biological Chemistry* **2013**, *288* (49), 35192–35209. https://doi.org/10.1074/jbc.M113.483727.

(10) Burkhart, B. W.; Febvre, H. P.; Santangelo, T. J. Distinct Physiological Roles of the Three Ferredoxins Encoded in the Hyperthermophilic Archaeon *Thermococcus Kodakarensis*. *mBio* **2019**, *10* (2). https://doi.org/10.1128/mBio.02807-18.

(11) Buckel, W.; Thauer, R. K. Flavin-Based Electron Bifurcation, A New Mechanism of Biological Energy Coupling. *Chem Rev* **2018**, *118* (7), 3862–3886. https://doi.org/10.1021/acs.chemrev.7b00707.

(12) Sétif, P. Ferredoxin and Flavodoxin Reduction by Photosystem I. *Biochimica et Biophysica Acta (BBA) - Bioenergetics* **2001**, *1507* (1–3), 161–179. https://doi.org/10.1016/S0005-2728(01)00205-5.

(13) Hall, D. O.; Cammack, R.; Rao, K. K. Role for Ferredoxins in the Origin of Life and Biological Evolution. *Nature* **1971**, *233* (5315), 136–138. https://doi.org/10.1038/233136a0.

(14) Capozzi, F.; Ciurli, S.; Luchinat, C. Coordination Sphere versus Protein Environment as Determinants of Electronic and Functional Properties of Iron-Sulfur Proteins. *Struct Bond* **1998**, *90*, 127–160.

(15) Stephens, P.; Jollie, D.; Warshel, A. Protein Control of Redox Potentials of Iron-Sulfur Proteins. *Chem Rev* **1996**, *96* (7), 2491–2514.

(16) Prince, R. C.; Adams, M. W. Oxidation-Reduction Properties of the Two Fe4S4 Clusters in Clostridium Pasteurianum Ferredoxin. *Journal of Biological Chemistry* **1987**, *262* (11), 5125–5128. https://doi.org/10.1016/S0021-9258(18)61163-9.

(17) Gao-Sheridan, H. S.; Pershad, H. R.; Armstrong, F. A.; Burgess, B. K. Discovery of a Novel Ferredoxin from Azotobacter Vinelandii Containing Two [4Fe-4S] Clusters with Widely Differing and Very Negative Reduction Potentials. *Journal of Biological Chemistry* **1998**, *273* (10), 5514–5519. https://doi.org/10.1074/jbc.273.10.5514.

(18) Saridakis, E.; Giastas, P.; Efthymiou, G.; Thoma, V.; Moulis, J. M.; Kyritsis, P.; Mavridis, I. M. Insight into the Protein and Solvent Contributions to the Reduction Potentials of [4Fe-4S]2+/+ Clusters: Crystal Structures of the Allochromatium Vinosum Ferredoxin Variants C57A and V13G and the Homologous Escherichia Coli Ferredoxin. *Journal of Biological Inorganic Chemistry* **2009**, *14* (5), 783–799. https://doi.org/10.1007/s00775-009-0492-x.

(19) Meyer, J. Ferredoxins of the Third Kind. *FEBS Lett* **2001**, *509* (1), 1–5. https://doi.org/10.1016/S0014-5793(01)03049-6.

(20) Tagawa, K.; Arnon, D. I. Ferredoxins as Electron Carriers in Photosynthesis and in the Biological Production and Consumption of Hydrogen Gas. *Nature* **1962**, *195* (4841), 537–543. https://doi.org/10.1038/195537a0.

(21) Lubitz, W.; Ogata, H.; Rüdiger, O.; Reijerse, E.; Rudiger, O.; Reijerse, E. Hydrogenases. *Chem Rev* **2014**, *114* (8), 4081–4148. https://doi.org/10.1021/cr4005814.

(22) Vignais, P. M.; Billoud, B. Occurrence, Classification, and Biological Function of Hydrogenases: An Overview. *Chem. Rev.* **2007**, *107* (10), 4206–4272. https://doi.org/10.1021/cr050196r.

(23) Tai, H.; Hirota, S.; Stripp, S. T. Proton Transfer Mechanisms in Bimetallic Hydrogenases. *Acc Chem Res* **2021**, *54* (1), 232–241. https://doi.org/10.1021/acs.accounts.0c00651.

(24) Nicolet, Y.; Piras, C.; Legrand, P.; Hatchikian, C. E.; Fontecilla-Camps, J. C. Desulfovibrio Desulfuricans Iron Hydrogenase: The Structure Shows Unusual Coordination to an Active Site Fe Binuclear Center. *Structure* **1999**, *7* (1), 13–23. https://doi.org/10.1016/S0969-2126(99)80005-7.

(25) Peters, J. W.; Lanzilotta, W. N.; Lemon, B. J.; Seefeldt, L. C. X-Ray Crystal Structure of the Fe-Only Hydrogenase (CpI) from Clostridium Pasteurianum to 1.8 Angstrom Resolution. *Science* **1998**, *282* (5395), 1853–1858. https://doi.org/10.1126/science.282.5395.1853.

(26) Esselborn, J.; Muraki, N.; Klein, K.; Engelbrecht, V.; Metzler-Nolte, N.; Apfel, U.-P.; Hofmann, E.; Kurisu, G.; Happe, T. A Structural View of Synthetic Cofactor Integration into [FeFe]-Hydrogenases. *Chem. Sci.* **2016**, *7*, 959–968. https://doi.org/10.1039/C5SC03397G.

(27) Stripp, S. T.; Duffus, B. R.; Fourmond, V.; Léger, C.; Leimkühler, S.; Hirota, S.; Hu, Y.; Jasniewski, A.; Ogata, H.; Ribbe, M. W. Second and Outer Coordination Sphere Effects in Nitrogenase, Hydrogenase, Formate Dehydrogenase, and CO Dehydrogenase. *Chem Rev* **2022**, *122* (14), 11900–11973. https://doi.org/10.1021/acs.chemrev.1c00914.

(28) Land, H.; Senger, M.; Berggren, G.; Stripp, S. T. Current State of [FeFe]-Hydrogenase Research - Biodiversity and Spectroscopic Investigations. *ACS Catal* **2020**, *10* (13), 7069–7086. https://doi.org/10.1021/acscatal.0c01614.

(29) Kleinhaus, J. T.; Wittkamp, F.; Yadav, S.; Siegmund, D.; Apfel, U.-P. [FeFe]-Hydrogenases: Maturation and Reactivity of Enzymatic Systems and Overview of Biomimetic Models. *Chem Soc Rev* **2021**, *50* (3), 1668–1784. https://doi.org/10.1039/D0CS01089H.

(30) Birrell, J. A.; Rodríguez-Maciá, P.; Reijerse, E. J.; Martini, M. A.; Lubitz, W. The Catalytic Cycle of [FeFe] Hydrogenase: A Tale of Two Sites. *Coord Chem Rev* **2021**, *449*, 214191. https://doi.org/10.1016/j.ccr.2021.214191.

(31) Yacoby, I.; Pochekailov, S.; Toporik, H.; Ghirardi, M. L.; King, P. W.; Zhang, S. Photosynthetic Electron Partitioning between [FeFe]-Hydrogenase and Ferredoxin:$NADP^+$-Oxidoreductase (FNR) Enzymes in Vitro. *Proceedings of the National Academy of Sciences* **2011**, *108* (23), 9396–9401. https://doi.org/10.1073/pnas.1103659108.

(32) Burkhart, B. W.; Febvre, H. P.; Santangelo, T. J. Distinct Physiological Roles of the Three Ferredoxins Encoded in the Hyperthermophilic Archaeon *Thermococcus Kodakarensis*. *mBio* **2019**, *10* (2). https://doi.org/10.1128/mBio.02807-18.

(33) Addison, H.; Glatter, T.; K. A. Hochberg, G.; Rebelein, J. G. Two Distinct Ferredoxins Are Essential for Nitrogen Fixation by the Iron Nitrogenase in *Rhodobacter Capsulatus*. *mBio* **2024**, *15* (3). https://doi.org/10.1128/mbio.03314-23.

(34) Artz, J. H.; Mulder, D. W.; Ratzloff, M. W.; Lubner, C. E.; Zadvornyy, O. A.; LeVan, A. X.; Williams, S. G.; Adams, M. W. W.; Jones, A. K.; King, P. W.; Peters, J. W. Reduction

Potentials of [FeFe]-Hydrogenase Accessory Iron–Sulfur Clusters Provide Insights into the Energetics of Proton Reduction Catalysis. *J Am Chem Soc* **2017**, *139* (28), 9544–9550. https://doi.org/10.1021/jacs.7b02099.

(35) Rumpel, S.; Siebel, J. F.; Diallo, M.; Farès, C.; Reijerse, E. J.; Lubitz, W. Structural Insight into the Complex of Ferredoxin and [FeFe] Hydrogenase from *Chlamydomonas Reinhardtii*. *ChemBioChem* **2015**, *16* (11), 1663–1669. https://doi.org/10.1002/cbic.201500130.

(36) Lubner, C. E.; Artz, J. H.; Mulder, D. W.; Oza, A.; Ward, R. J.; Williams, S. G.; Jones, A. K.; Peters, J. W.; Smalyukh, I. I.; Bharadwaj, V. S.; King, P. W. A Site-Differentiated [4Fe–4S] Cluster Controls Electron Transfer Reactivity of *Clostridium Acetobutylicum* [FeFe]-Hydrogenase I. *Chem Sci* **2022**, *13* (16), 4581–4588. https://doi.org/10.1039/D1SC07120C.

(37) Kozakov, D.; Hall, D. R.; Xia, B.; Porter, K. A.; Padhorny, D.; Yueh, C.; Beglov, D.; Vajda, S. The ClusPro Web Server for Protein-Protein Docking. *Nat Protoc* **2017**, *12* (2), 255–278. https://doi.org/10.1038/nprot.2016.169.

(38) Barth, A. Infrared Spectroscopy of Proteins. *Biochimica et Biophysica Acta (BBA) - Bioenergetics* **2007**, *1767* (9), 1073–1101. https://doi.org/10.1016/j.bbabio.2007.06.004.

(39) Mäntele, W. Reaction-Induced Infrared Difference Spectroscopy for the Study of Protein Function and Reaction Mechanisms. *Trends Biochem Sci* **1993**, *18* (6), 197–202. https://doi.org/10.1016/0968-0004(93)90186-Q.

(40) Kötting, C.; Gerwert, K. Proteins in Action Monitored by Time-Resolved FTIR Spectroscopy. *ChemPhysChem* **2005**, *6* (5), 881–888. https://doi.org/10.1002/cphc.200400504.

(41) Kottke, T.; Lórenz-Fonfría, V. A.; Heberle, J. The Grateful Infrared: Sequential Protein Structural Changes Resolved by Infrared Difference Spectroscopy. *J Phys Chem B* **2017**, *121* (2), 335–350. https://doi.org/10.1021/acs.jpcb.6b09222.

(42) Lórenz-Fonfria, V. A. Infrared Difference Spectroscopy of Proteins: From Bands to Bonds. *Chem Rev* **2020**, *120* (7), 3466–3576. https://doi.org/10.1021/acs.chemrev.9b00449.

(43) Stripp, S. T. In Situ Infrared Spectroscopy for the Analysis of Gas-Processing Metalloenzymes. *ACS Catal* **2021**, *11* (13), 7845–7862. https://doi.org/10.1021/acscatal.1c00218.

(44) Sahin, S.; Milton, R. D. Evolving Enzymatic Electrochemistry with Rare or Unnatural Amino Acids. *Curr Opin Electrochem* **2022**, *35*, 101102. https://doi.org/10.1016/j.coelec.2022.101102.

(45) Kim, H.; Cho, M. Infrared Probes for Studying the Structure and Dynamics of Biomolecules. *Chem Rev* **2013**, *113* (8), 5817–5847. https://doi.org/10.1021/cr3005185.

(46) Fried, S. D.; Boxer, S. G. Measuring Electric Fields and Noncovalent Interactions Using the Vibrational Stark Effect. *Acc Chem Res* **2015**, *48* (4), 998–1006. https://doi.org/10.1021/ar500464j.

(47) Fried, S. D.; Boxer, S. G. Electric Fields and Enzyme Catalysis. *Annu Rev Biochem* **2017**, *86* (1), 387–415. https://doi.org/10.1146/annurev-biochem-061516-044432.

(48) Park, E. S.; Andrews, S. S.; Hu, R. B.; Boxer, S. G. Vibrational Stark Spectroscopy in Proteins: A Probe and Calibration for Electrostatic Fields. *J Phys Chem B* **1999**, *103* (45), 9813–9817. https://doi.org/10.1021/jp992329g.

(49) Weaver, J. B.; Kozuch, J.; Kirsh, J. M.; Boxer, S. G. Nitrile Infrared Intensities Characterize Electric Fields and Hydrogen Bonding in Protic, Aprotic, and Protein Environments. *J Am Chem Soc* **2022**, *144* (17), 7562–7567. https://doi.org/10.1021/jacs.2c00675.

(50) Kuznetsov, G.; Goodman, D. B.; Filsinger, G. T.; Landon, M.; Rohland, N.; Aach, J.; Lajoie, M. J.; Church, G. M. Optimizing Complex Phenotypes through Model-Guided Multiplex Genome Engineering. *Genome Biol* **2017**, *18* (1), 100. https://doi.org/10.1186/s13059-017-1217-z.

(51) Miyake-Stoner, S. J.; Miller, A. M.; Hammill, J. T.; Peeler, J. C.; Hess, K. R.; Mehl, R. A.; Brewer, S. H. Probing Protein Folding Using Site-Specifically Encoded Unnatural Amino Acids as FRET Donors with Tryptophan. *Biochemistry* **2009**, *48* (25), 5953–5962. https://doi.org/10.1021/bi900426d.

(52) Miyake-Stoner, S. J.; Refakis, C. A.; Hammill, J. T.; Lusic, H.; Hazen, J. L.; Deiters, A.; Mehl, R. A. Generating Permissive Site-Specific Unnatural Aminoacyl-TRNA Synthetases. *Biochemistry* **2010**, *49* (8), 1667–1677. https://doi.org/10.1021/bi901947r.

(53) Kuchenreuther, J. M.; Grady-Smith, C. S.; Bingham, A. S.; George, S. J.; Cramer, S. P.; Swartz, J. R. High-Yield Expression of Heterologous [FeFe] Hydrogenases in Escherichia Coli. *PLoS One* **2010**, *5* (11), e15491. https://doi.org/10.1371/journal.pone.0015491.

(54) Schönheit, P.; Wäscher, C.; Thauer, R. K. A Rapid Procedure for the Purification of Ferredoxin from Clostridia Using Polyethyleneimine. *FEBS Lett* **1978**, *89* (2), 219–222. https://doi.org/10.1016/0014-5793(78)80221-X.

(55) Britt, R. D.; Rao, G.; Tao, L. Biosynthesis of the Catalytic H-Cluster of [FeFe] Hydrogenase: The Roles of the Fe–S Maturase Proteins HydE, HydF, and HydG. *Chem Sci* **2020**, *11* (38), 10313–10323. https://doi.org/10.1039/D0SC04216A.

(56) Urquidi, O.; Brazard, J.; LeMessurier, N.; Simine, L.; Adachi, T. B. M. In Situ Optical Spectroscopy of Crystallization: One Crystal Nucleation at a Time. *Proceedings of the National Academy of Sciences* **2022**, *119* (16). https://doi.org/10.1073/pnas.2122990119.

(57) Stripp, S. T.; Goldet, G.; Brandmayr, C.; Sanganas, O.; Vincent, K. A.; Haumann, M.; Armstrong, F. A.; Happe, T. How Oxygen Attacks [FeFe] Hydrogenases from Photosynthetic Organisms. *Proc Natl Acad Sci U S A* **2009**, *106* (41), 17331–17336. https://doi.org/10.1073/pnas.0905343106.

(58) Tsibris, J. C. M.; Woody, R. W. Structural Studies of Iron-Sulfur Proteins. *Coord Chem Rev* **1970**, *5* (4), 417–458. https://doi.org/10.1016/S0010-8545(00)80100-9.

(59) Tucker, M. J.; Oyola, R.; Gai, F. Conformational Distribution of a 14-Residue Peptide in Solution: A Fluorescence Resonance Energy Transfer Study. *J Phys Chem B* **2005**, *109* (10), 4788–4795. https://doi.org/10.1021/jp044347q.

(60) Ries, L. K.; Schmid, F. X.; Schmidpeter, P. A. M. Incorporation of an Unnatural Amino Acid as a Domain-Specific Fluorescence Probe in a Two-Domain Protein. *Biochemistry* **2016**, *55* (49), 6739–6742. https://doi.org/10.1021/acs.biochem.6b00898.

(61) Armstrong, F. A.; Camba, R.; Heering, H. A.; Hirst, J.; Jeuken, L. J. C.; Jones, A. K.; Le′ger, C.; McEvoy, J. P. Fast Voltammetric Studies of the Kinetics and Energetics of Coupled Electron-Transfer Reactions in Proteins. *Faraday Discuss* **2000**, *116*, 191–203. https://doi.org/10.1039/b002290j.

(62) Milton, R. D.; Ruth, J. C.; Deutzmann, J. S.; Spormann, A. M. *Methanococcus Maripaludis* Employs Three Functional Heterodisulfide Reductase Complexes for Flavin-Based Electron Bifurcation Using Hydrogen and Formate. *Biochemistry* **2018**, *57* (32), 4848–4857. https://doi.org/10.1021/acs.biochem.8b00662.

(63) Therien, J. B.; Artz, J. H.; Poudel, S.; Hamilton, T. L.; Liu, Z.; Noone, S. M.; Adams, M. W. W.; King, P. W.; Bryant, D. A.; Boyd, E. S.; Peters, J. W. The Physiological Functions and Structural Determinants of Catalytic Bias in the [FeFe]-Hydrogenases CpI and CpII of Clostridium Pasteurianum Strain W5. *Front Microbiol* **2017**, *8* (JUL), 1–11. https://doi.org/10.3389/fmicb.2017.01305.

(64) Khushvakov, J.; Nussbaum, R.; Cadoux, C.; Duan, J.; Stripp, S. T.; Milton, R. D. Following Electroenzymatic Hydrogen Production by Rotating Ring Disk Electrochemistry and Mass Spectrometry. *Angewandte Chemie - International Edition* **2021**, *60* (18), 10001–10006. https://doi.org/https://doi.org/10.1002/anie.202100863.

(65) Suydam, I. T.; Boxer, S. G. Vibrational Stark Effects Calibrate the Sensitivity of Vibrational Probes for Electric Fields in Proteins. *Biochemistry* **2003**, *42* (41), 12050–12055. https://doi.org/10.1021/bi0352926.

(66) Stripp, S. T.; Happe, T. How Algae Produce Hydrogen - News from the Photosynthetic Hydrogenase. *Dalton transactions* **2009**, *45*, 9960–9969. https://doi.org/10.1039/b916246a.

(67) Gauquelin, C.; Baffert, C.; Richaud, P.; Kamionka, E.; Etienne, E.; Guieysse, D.; Girbal, L.; Fourmond, V.; André, I.; Guigliarelli, B.; Léger, C.; Soucaille, P.; Meynial-Salles, I. Roles of the F-Domain in [FeFe] Hydrogenase. *Biochim Biophys Acta Bioenerg* **2018**, *1859* (2), 69–77. https://doi.org/10.1016/j.bbabio.2017.08.010.

(68) Girbal, L.; Von Abendroth, G.; Winkler, M.; Benton, P.; Meynial-Salles, I.; Croux, C.; Peters, J. W.; Happe, T.; Soucaille, P. Homologous and Heterologous Overexpression in Clostridium Acetobutylicum and Characterization of Purified Clostridial and Algal Fe-Only Hydrogenases with High Specific Activities. *Appl Environ Microbiol* **2005**, *71* (5), 2777–2781. https://doi.org/10.1128/AEM.71.5.2777.

(69) Ohki, S.; Kainosho, M. Stable Isotope Labeling Methods for Protein NMR Spectroscopy. *Prog Nucl Magn Reson Spectrosc* **2008**, *53* (4), 208–226. https://doi.org/10.1016/j.pnmrs.2008.01.003.

(70) Fafarman, A. T.; Boxer, S. G. Nitrile Bonds as Infrared Probes of Electrostatics in Ribonuclease S. *J Phys Chem B* **2010**, *114* (42), 13536–13544. https://doi.org/10.1021/jp106406p.

(71) Adesina, A. S.; Świderek, K.; Luk, L. Y. P.; Moliner, V.; Allemann, R. K. Electric Field Measurements Reveal the Pivotal Role of Cofactor–Substrate Interaction in Dihydrofolate Reductase Catalysis. *ACS Catal* **2020**, *10* (14), 7907–7914. https://doi.org/10.1021/acscatal.0c01856.

(72) Suydam, I. T.; Snow, C. D.; Pande, V. S.; Boxer, S. G. Electric Fields at the Active Site of an Enzyme: Direct Comparison of Experiment with Theory. *Science* **2006**, *313* (5784), 200–204. https://doi.org/10.1126/science.1127159.

(73) Dong, Y.; Zhang, S.; Wu, Z.; Li, X.; Wang, W. L.; Zhu, Y.; Stoilova-McPhie, S.; Lu, Y.; Finley, D.; Mao, Y. Cryo-EM Structures and Dynamics of Substrate-Engaged Human 26S Proteasome. *Nature* **2019**, *565* (7737), 49–55. https://doi.org/10.1038/s41586-018-0736-4.

(74) Shvarev, D.; Januliene, D.; Moeller, A. Frozen Motion: How Cryo-EM Changes the Way We Look at ABC Transporters. *Trends Biochem Sci* **2022**, *47* (2), 136–148. https://doi.org/10.1016/j.tibs.2021.11.008.

(75) Rutledge, H. L.; Cook, B. D.; Nguyen, H. P. M.; Herzik, M. A.; Tezcan, F. A. Structures of the Nitrogenase Complex Prepared under Catalytic Turnover Conditions. *Science (1979)* **2022**, *377* (6608), 865–869. https://doi.org/10.1126/science.abq7641.

(76) Steinhilper, R.; Freibert, S.-A.; Kaltwasser, S.; Lill, R.; Murphy, B. J. Structural Evidence for Two-Stage Binding of Mitochondrial Ferredoxin 2 to the Core Iron-Sulfur Cluster Assembly Complex. *BioRxiv* **2024**. https://doi.org/10.1101/2024.02.19.580858.

(77) Page, C. C.; Moser, C. C.; Chen, X.; Dutton, P. L. Natural Engineering Principles of Electron Tunnelling in Biological Oxidation-Reduction. *Nature* **1999**, *402* (6757), 47–52. https://doi.org/10.1038/46972.

(78) Rodríguez-Maciá, P.; Breuer, N.; DeBeer, S.; Birrell, J. A. Insight into the Redox Behavior of the [4Fe–4S] Subcluster in [FeFe] Hydrogenases. *ACS Catal* **2020**, *10* (21), 13084–13095. https://doi.org/10.1021/acscatal.0c02771.

TABLE OF CONTENTS

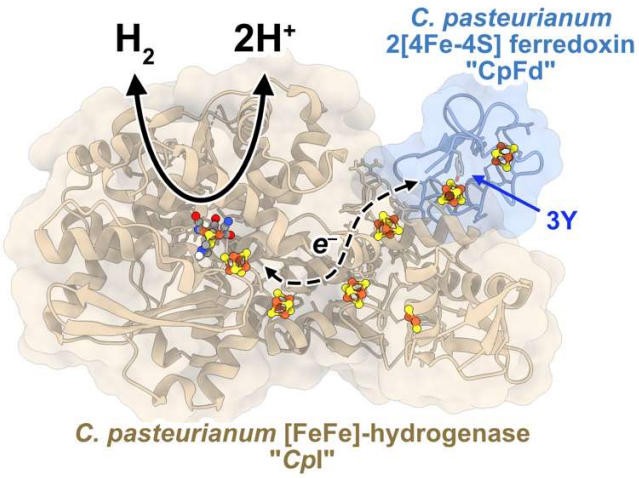

The electron transfer complex of [FeFe]-hydrogenase *Cp*I and ferredoxin *Cp*Fd was probed under reducing or oxidizing conditions. Time-resolved infrared spectroscopy indicates structural changes that modulate redox-dependent protein-protein interaction.